CrossMark

Evidence for Enrichment of Niobium-92 in the Outer Protosolar Disk

Yuki Hibiya[1] , Tsuyoshi Iizuka[2] , Hatsuki Enomoto[2], and Takehito Hayakawa[3]

[1] Research Center for Advanced Science and Technology, The University of Tokyo, 4-6-1 Komaba, Meguro-ku, Tokyo 153-8904, Japan
yuki-hibiya@g.ecc.u-tokyo.ac.jp

[2] Department of Earth and Planetary Science, The University of Tokyo, 7-3-1 Hongo, Bunkyo-ku, Tokyo 113-0033, Japan

[3] National Institutes for Quantum Science and Technology, 2-4 Shirakata, Tokai, Naka, Ibaraki 319-1106, Japan

Abstract

The short-lived radionuclide, niobium-92 (^{92}Nb), has been used to estimate the site of nucleosynthesis for p-nuclei and the timing of planetary differentiation, assuming that it was uniformly distributed in the early solar system. Here, we present the internal niobium–zirconium (Nb–Zr) isochron dating of Northwest Africa (NWA) 6704, an achondrite thought to form in the outer protosolar disk due to nucleosynthetic isotope similarities with carbonaceous chondrites. The isochron defines an initial ^{92}Nb/^{93}Nb ratio of $(2.72 \pm 0.25) \times 10^{-5}$ at the NWA 6704 formation, 4562.76 ± 0.30 million years ago. This corresponds to a ^{92}Nb/^{93}Nb ratio of $(2.96 \pm 0.27) \times 10^{-5}$ at the time of solar system formation, which is $\sim 80\%$ higher than the values obtained from meteorites formed in the inner disk. The results suggest that a significant proportion of the solar ^{92}Nb was produced by a nearby core-collapse supernova (CCSN) and that the outer disk was more enriched in CCSN ejecta, which could account for the heterogeneity of short-lived ^{26}Al and nucleosynthetic stable-isotope anomalies across the disk. We propose that NWA 6704 serves as the best anchor for mapping relative Nb–Zr ages of objects in the outer solar system onto the absolute timescale.

Unified Astronomy Thesaurus concepts: Nucleosynthesis (1131); Solar system formation (1530); Supernovae (1668); Meteorites (1038)

1. Introduction

Meteorites contain isotope evidence that short-lived radionuclides (SLRs) were extant in the early solar system. Understanding the origin of these SLRs has important implications for the stellar environment and the timeline of the solar system formation. The SLR niobium-92 (^{92}Nb), which decays to ^{92}Zr with a mean life (τ) of 53 million years (Myr; Holden 1990), is of particular interest. Unlike the majority of the SLRs, ^{92}Nb is a proton-rich nuclide that cannot be produced by slow or rapid neutron capture reactions (s- or r-process). Instead, ^{92}Nb is synthesized through nuclear reactions that occur during supernova explosions. However, the nucleosynthetic process and the nature of supernova progenitors remain controversial. Once the nucleosynthetic origin is understood, ^{92}Nb can be used to examine late-stage presolar supernova activity and its potential role in the formation of our solar system. As Nb and zirconium (Zr) are both refractory and fractionated during silicate differentiation and core formation (Jochum et al. 1986; Münker et al. 2017), ^{92}Nb can also be used as a chronometer for planetary differentiation. To determine its origin and validate its use as a chronometer, the initial abundance of ^{92}Nb and its distribution in the solar system must be established.

The first evidence for live ^{92}Nb in the early solar system was provided by a ^{92}Zr excess detected in a Nb-rich rutile of the Toluca iron meteorite (Harper 1996). Subsequently, the Zr isotope variation in single meteoritic phases containing fractionated Nb/Zr, such as zircon and Ca–Al-rich inclusions (CAIs), was investigated (Münker et al. 2000; Sanloup et al. 2000;

Yin et al. 2000; Hirata 2001; Schönbächler et al. 2003). However, in order to determine the initial abundance and distribution of ^{92}Nb, the internal Nb–Zr isochrons for multiple meteorites with known absolute ages must be obtained. Therefore, internal Nb–Zr isochron dating has been applied to basaltic achondrites, ordinary chondrites, and mesosiderites with known absolute U–Pb ages (Schönbächler et al. 2002; Iizuka et al. 2016; Haba et al. 2021). The results revealed the uniform distribution of ^{92}Nb relative to the stable isotope ^{93}Nb in the source regions of these meteorites, with mesosiderites providing the most precise estimate for ^{92}Nb/^{93}Nb at the time of CAI formation $(^{92}$Nb/^{93}Nb$)_0$ of $(1.66 \pm 0.10) \times 10^{-5}$ (Haba et al. 2021).

Northwest Africa (NWA) 6704, a unique meteorite, is an unbrecciated achondrite with a broadly chondritic bulk composition, which likely formed by impact melting on an undifferentiated asteroid (Hibiya et al. 2019). This meteorite is well suited for determining the initial SLR abundances of the solar system because, (i) its absolute age has been precisely determined to be 4562.76 ± 0.30 Myr using the U–Pb method (Amelin et al. 2019); (ii) its antiquity combined with its diverse mineral assemblage allows for the determination of precise internal isochrons of various SLR decay systems, including ^{92}Nb–^{92}Zr, ^{53}Mn–^{53}Cr ($\tau = 5.3$ Myr), and ^{26}Al–^{26}Mg ($\tau = 1.0$ Myr); and (iii) the closure of the U–Pb and SLR decay systems can be regarded as concurrent due to the rapid cooling during crystallization and lack of evidence for significant postcrystallization processes (Hibiya et al. 2019). In addition, NWA 6704 shows excess of ^{50}Ti, ^{46}Ti, and ^{54}Cr relative to Earth (Hibiya et al. 2019; Sanborn et al. 2019), which are within the ranges measured for carbonaceous chondrites. This is in striking contrast to ordinary and enstatite chondrites, as well as a majority of achondrites, which exhibit deficits in these isotopes. The isotope dichotomy between noncarbonaceous and carbonaceous

meteorites is thought to reflect a fundamental difference in the contribution of a nucleosynthetic component between the inner and outer protosolar disks in which the former and latter parent bodies have formed, respectively (Leya et al. 2008; Warren 2011). As all previously Nb–Zr-dated meteorites have ^{50}Ti and ^{46}Ti deficits, Nb–Zr dating of the NWA 6704 "carbonaceous" achondrite significantly adds to understanding of the ^{92}Nb distribution in the protosolar disk. In this study, we present internal Nb–Zr isochron dating of NWA 6704 and demonstrated that while ^{92}Nb was homogeneously distributed within the inner disk, its abundance was distinctly higher in the outer disk.

2. Materials and Methods

We prepared mineral and whole-rock fractions (four orthopyroxene, one metal, six chromite, and two whole-rock fractions) from five NWA 6704 fragments. All fragments were crushed using an agate mortar and pestle. Whole-rock fractions were extracted directly from crushed samples. The nonmagnetic mineral fractions were handpicked from the samples, whereas the metal fraction was separated using a neodymium hand magnet. All nonmagnetic mineral fractions were digested with a mixture of concentrated HF and HNO_3, whereas the metal fraction was digested with reverse aqua regia and the HCl–HF mixture. Finally, all fractions were redissolved in 6 mol L^{-1} HCl. Each digested solution was split into two aliquots for the determination of the ^{93}Nb/^{90}Zr ratio (2%–10%) and Zr isotope composition (90%–98%). Aliquots for the Zr isotope analyses were purified using ion-exchange chemistry, whereas those for ^{93}Nb/^{90}Zr analyses were not processed for chemical separation in order to avoid artificial Nb/Zr fractionation. We analyzed the Zr isotope compositions and ^{93}Nb/^{90}Zr of the sample aliquots using a Thermo Fisher Scientific Neptune Plus MC-ICP–MS interfaced to a Cetac Aridus II desolvating nebulizer and iCAP Q ICP–MS, respectively. The analytical methods are described in detail in the Appendix.

3. Results

The ^{91}Zr/^{90}Zr values in all fractions are indistinguishable from the terrestrial standard, but the ^{96}Zr/^{90}Zr values are higher, with a mean ε^{96}Zr value of 1.54 ± 0.84 (the ε notations represent deviations from the terrestrial ratios in parts per 10^4; Table A1). Such a prominent ε^{96}Zr excess has been detected in carbonaceous chondrites (Akram et al. 2015; Render et al. 2022), supporting the NWA 6704 parent body formed in the outer protosolar disk. There are no resolvable anomalies in the orthopyroxene, metal, or whole-rock fractions with respect to the ^{92}Zr/^{90}Zr ratio. In contrast, the chromite fractions show elevated ^{92}Zr/^{90}Zr, with ε^{92}Zr values ranging from +0.56 to +1.51, which correlate well with the ^{93}Nb/^{90}Zr (Figure 1). There is no linear correlation between ε^{92}Zr and the reciprocal of Zr concentration (Figure 2), demonstrating that the regression line in Figure 1 is an isochron rather than a mixing line. Thus, the y-intercept of the regression line defines an initial ε^{92}Zr of –0.16 ± 0.09, and the slope defines an initial ^{92}Nb/^{93}Nb of (2.72 ± 0.25) × 10^{-5} at the time of NWA 6704 formation.
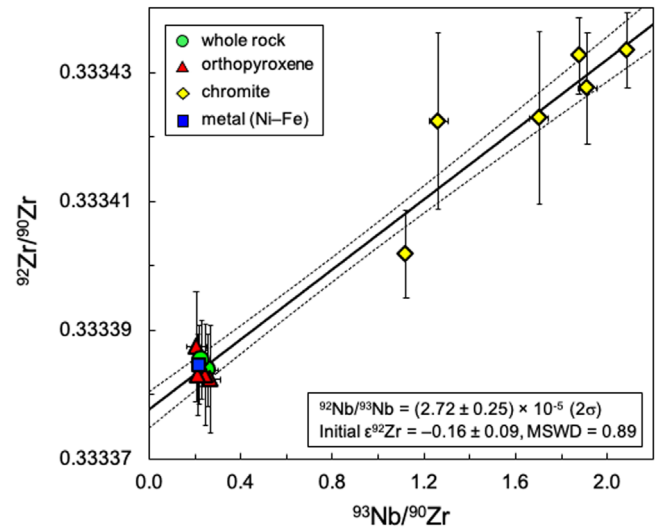

Figure 1. Nb–Zr isochron diagram for NWA 6704. The error bars reflect 2σ. Solid and dashed lines represent the isochron and error envelopes (at 95% confidence) based on the regression of the data, respectively. For the isochron regression, all ^{92}Zr/^{90}Zr were normalized to ^{92}Zr/^{90}Zr = 0.333383 for the standard solution, following previous studies (Schönbächler et al. 2002; Iizuka et al. 2016).

4. Discussion

Combining the obtained initial ^{92}Nb/^{93}Nb of (2.72 ± 0.25) × 10^{-5} at the time of NWA 6704 formation with the U–Pb age of 4562.76 ± 0.30 Myr (Amelin et al. 2019), we derive a ^{92}Nb/^{93}Nb at the time of CAI formation $(^{92}$Nb/^{93}Nb$)_0$ of (2.96 ± 0.27) × 10^{-5}. This value is significantly higher than the $(^{92}$Nb/^{93}Nb$)_0$ values of ~1.7 × 10^{-5} defined by the angrite NWA 4590, eucrite Agoult, and mesosiderites (Schönbächler et al. 2002; Iizuka et al. 2016; Haba et al. 2021; Figure 3). Considering that NWA 6704 and previously Nb–Zr dated meteorites represent samples of the outer and inner protosolar disks, respectively, our results indicate that ^{92}Nb was heterogeneously distributed across the disk. The enrichment of ^{92}Nb in the outer disk is consistent with the observation that bulk carbonaceous meteorites have higher ^{92}Zr/^{90}Zr ratios than noncarbonaceous ones (Render et al. 2022).

The finding provides new insights into the nucleosynthetic origin of ^{92}Nb. Thermonuclear and core-collapse supernovae (CCSNe) have been proposed as potential stellar sources of ^{92}Nb. In thermonuclear Type Ia supernovae (SNe Ia), ^{92}Nb could be synthesized by photodisintegration reactions (γ-process; Travaglio et al. 2014), whereas in CCSNe, it could be produced by the γ-process (Dauphas et al. 2003) reactions in the freezeout of equilibrium in the presence of α particles (α-rich freezeout; Meyer 2003; Lugaro et al. 2016), and reactions induced by energetic neutrinos (ν-process; Hayakawa et al. 2013; Sieverding et al. 2018). A simulation of galactic chemical evolution (GCE; Travaglio et al. 2014) predicts that if nucleosynthesis occurs only in SNe Ia, the steady-state abundance ratio of ^{92}Nb to a stable p-process nuclide ^{92}Mo in the interstellar medium (ISM) would be (1.72 +1.40/−0.06) × 10^{-5}. The predicted value has only a slight overlap with an initial solar ^{92}Nb/^{92}Mo ratio of (3.3 ± 0.2) × 10^{-5} calculated from the $(^{92}$Nb/^{93}Nb$)_0$ defined by mesosiderites (Haba et al. 2021) and the solar Mo/Nb of 3.27 (Lodders et al. 2009). It follows that if ^{92}Nb is produced solely in SNe Ia, our solar system must be formed immediately after the protosolar molecular cloud isolation from the ISM. However,
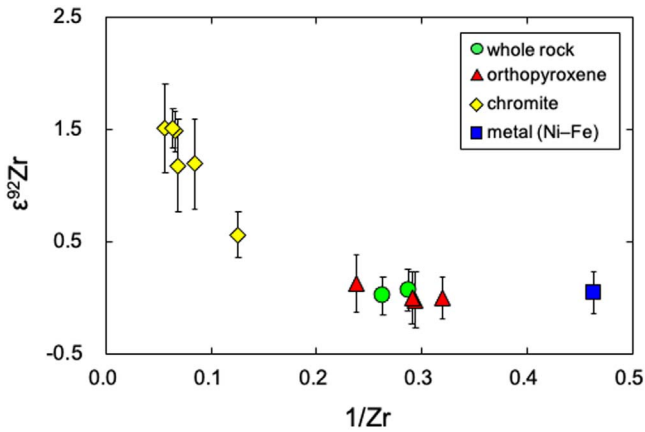
Figure 2. Plot of ε^{92}Zr vs. $1/$Zr for the whole-rock and mineral fractions of the NWA 6704 achondrite. Error bars represent 2σ, as listed in Table A1.

such a short isolation timescale contradicts estimates from other SLRs such as ^{53}Mn, ^{146}Sm, and ^{182}Hf (Lugaro et al. 2014, 2016; Haba et al. 2021), suggesting that ^{92}Nb was produced not only by SNe Ia but also by CCSNe. Our newly defined $(^{92}$Nb/^{93}Nb$)_0$ using NWA 6704 yielded an initial ^{92}Nb/^{92}Mo value of $(6.3 \pm 0.6) \times 10^{-5}$ for the outer solar system. Hence, the bulk solar system represented by carbonaceous meteorites should have a distinctly higher ^{92}Nb/^{92}Mo value than predicted by Travaglio et al. (2014), strengthening the contribution of CCSNe to the ^{92}Nb production.

A CCSN-derived SLR in the early solar system could be either inherited from the ambient ISM or newly produced by the explosion of a local massive star in the protosolar molecular cloud. The latter self-pollution scenario has been invoked to account for the solar initial abundance of the SLR ^{26}Al that is clearly higher than the astronomically observed galactic ISM background level (Diehl et al. 2006), though whether the source is a CCSN or Wolf–Rayet star remains debatable (Meyer 2005; Sahijpal & Soni 2006; Gaidos et al. 2009; Tatischeff et al. 2010; Young 2016; Dwarkadas et al. 2017). Due to the extremely low probability of such an encounter, the self-pollution by an asymptotic giant branch star (AGB; Wasserburg et al. 2006) or SN Ia is generally discounted (Kastner & Myers 1994; Huss et al. 2009). Notably, Al–Mg dating of meteoritic samples with known absolute ages (Schiller et al. 2015; Bollard et al. 2019; Sanborn et al. 2019; Wimpenny et al. 2019) indicated a lower initial abundance of ^{26}Al in the inner than the outer protosolar disk, which is comparable to the ^{92}Nb heterogeneity. This is in contrast to the homogenous distribution of the SLRs ^{53}Mn, ^{146}Sm, and ^{182}Hf (Kleine et al. 2012; Sanborn et al. 2019; Fang et al. 2022) that are considered to have other stellar origins such as AGB stars and SNe Ia (Holst et al. 2013; Lugaro et al. 2014, 2016; Côté et al. 2019). These observations suggest that the outer protosolar disk was more polluted by ejecta from a nearby CCSN, including newly synthesized ^{26}Al and ^{92}Nb.

The enrichment of such CCSN ejecta in the outer disk could explain the Cr–Ti stable-isotope dichotomy between carbonaceous and noncarbonaceous meteorites. The enrichments of ^{54}Cr, ^{50}Ti, and ^{46}Ti in carbonaceous chondrites can be attributed to the addition of a component synthesized by the weak s-process in a massive star during pre-CCSN stages (Qin et al. 2011a). As CCSN explosions eject a weak s-process component, these stable-isotope variations in the protosolar disk are expected to

be associated with changes in the initial abundances of ^{26}Al and ^{92}Nb if the explosion occurred shortly before or during solar system formation.

Due to the ^{92}Nb heterogeneity across the protosolar disk, the ^{92}Nb clock must be calibrated for dating early solar system events. The direct use of an SLR as an early solar system chronometer is based on the assumption that its initial abundance was uniform across the sample source regions. The nonuniformity leads to erroneous relative ages, which can be corrected if the initial abundance difference is known. Our results show that the $(^{92}$Nb/^{93}Nb$)_0$ in the source region of the "carbonaceous" achondrite NWA 6704 was $\sim$80% higher than those of the ordinary chondrites, angrite, eucrite, and mesosiderites. If the Nb–Zr ages of samples that formed in the outer disk were estimated using the inner solar system $(^{92}$Nb/^{93}Nb$)_0$ value, a correction of up to 30 Myr would be required. Furthermore, given that the building blocks of the terrestrial planets are derived from both the inner and outer disk (Schiller et al. 2018), neither the inner solar system nor our newly defined $(^{92}$Nb/^{93}Nb$)_0$ value are appropriate for Nb–Zr dating of differentiation in the planets. As the timing of early Nb/Zr differentiation on a given planet depends on its $(^{92}$Nb/^{93}Nb$)_0$ being adopted, an appropriate initial ratio must be determined by using a tracer that reflects the bulk composition of the building blocks. Candidates for such a tracer would be the nucleosynthetic stable-isotope variations that were generated by the same stellar source as the ^{92}Nb heterogeneity.

5. Conclusion

We conducted Nb–Zr isotopic analysis on the NWA 6704 achondrite that is considered to have originated from the formation region of carbonaceous chondrites. The obtained internal isochron defines an initial ^{92}Nb/^{93}Nb ratio of $(2.72 \pm 0.25) \times 10^{-5}$ at the time of NWA 6704 formation. By combining this value with the U–Pb age of NWA 6704, a $(^{92}$Nb/^{93}Nb$)_0$ ratio of $(2.96 \pm 0.27) \times 10^{-5}$ at the time of solar system formation was derived. The value is significantly higher than previous estimates based on noncarbonaceous meteorites, indicating that ^{92}Nb was more abundant in the outer protosolar disk than the inner. Our newly obtained initial ^{92}Nb/^{93}Nb value is clearly higher than the expected galactic background produced solely by SNe Ia, requiring that ^{92}Nb has a CCSN origin. Given that SLRs inherited from the ISM were homogeneously distributed in the protosolar disk, the ^{92}Nb heterogeneity suggests that a nearby CCSN contributed significantly to ^{92}Nb production. The enrichment of such CCSN ejecta in the outer disk could explain the enigmatic heterogeneity of ^{26}Al and nucleosynthetic stable-isotope anomalies in the disk. We propose NWA 6704 as a time anchor to map the Nb–Zr relative ages of objects in the outer solar system objects onto the absolute timescale.
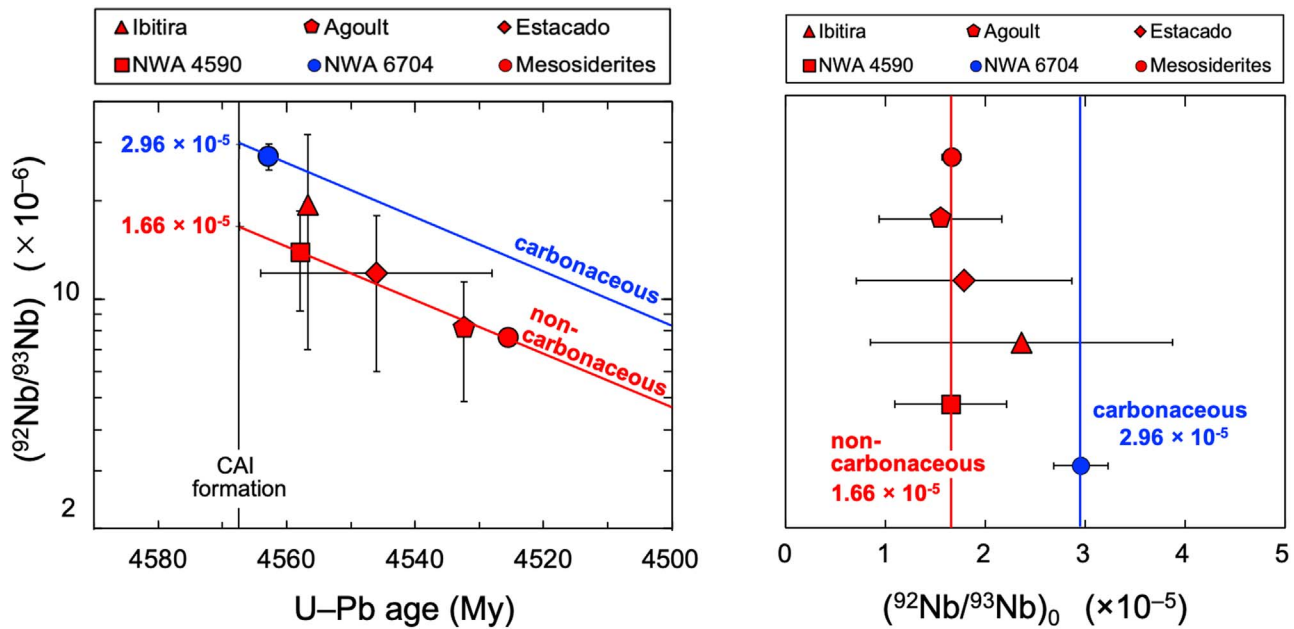
Figure 3. Comparison of the initial ^{92}Nb/^{93}Nb ratios of the meteorites. (a) Initial ^{92}Nb/^{93}Nb vs. U–Pb age plots for the meteorites. (b) ^{92}Nb/^{93}Nb ratios at the time of CAI formation (4567.3 Myr; Connelly et al. [2012]), (^{92}Nb/^{93}Nb)$_0$, derived from the meteorites. The data are from this study and Schönbächler et al. [2002], Iizuka et al. [2016], and Haba et al. [2021] for the initial ^{92}Nb/^{93}Nb ratios and Amelin et al. [2019], Blinova et al. [2007], Iizuka et al. [2019], Brennecka et al. [2020], Iizuka et al. [2014], and Haba et al. [2019] for data for the U–Pb ages. All errors represent 2σ. The red and blue lines represent the ^{92}Nb/^{93}Nb decay curves passing through the data points of the "noncarbonaceous" mesosiderites and "carbonaceous" meteorite NWA 6704, yielding (^{92}Nb/^{93}Nb)$_0$ of $(1.66 \pm 0.10) \times 10^{-5}$ and $(2.96 \pm 0.27) \times 10^{-5}$, respectively.

implications. Competing interests: The authors declare no conflicts of interest. Data and materials availability: All data can be found in the main text or the Appendix.

Appendix

A.1. Analytical Procedures

A.1.1. Sample Digestion

We prepared mineral and whole-rock fractions from five fragments of NWA 6704 (in total 10 g): two ∼50 mg of whole-rock fractions from fragment #1; two 40–50 mg orthopyroxene fractions and two ∼4 mg chromite fractions from fragment #2; one ∼30 mg orthopyroxene fraction and one ∼3 mg chromite fraction from fragment #3; one 50 mg orthopyroxene fraction, two ∼7 mg chromite fractions, and one ∼165 mg metal fraction from fragment #4; and one ∼7 mg chromite fraction from fragment #5.

All nonmagnetic mineral fractions were digested with a mixture of concentrated HF and HNO$_3$ in Teflon vials inside a Parr bomb at 210°C. The metal fraction was digested in a Teflon vial at 140°C by treating it with reverse aqua regia (concentrated HNO$_3$:concentrated HCl = 2:1) and the HCl–HF mixtures, that is, by using a modified version of a previously reported method (Cook et al. [2008]).

### A.1.2. Chemical Purification of Zr

For high-precision Zr isotope ratio measurements, the removal of elements that could cause spectral interferences is crucial. During Zr isotope analysis based on multiple collector inductively coupled plasma mass spectrometry (MC-ICP–MS), problematic interferences arise from isobaric ions of Mo and Ru (Figure A1) and argide ions of Fe, Cr, and Ti (Figure A2). In this study, Zr was purified using a two-step ion-exchange

procedure based on previous reports (Münker et al. [2001]; Iizuka et al. [2016]; Table A2). In the first step, Fe was separated from other elements, including Zr, using a column packed with 2 mL of Bio-Rad AG1-X8 anion exchange resin (200–400 mesh) in which Zr was eluted with ∼6 mL of 6 mol L^{-1} HCl, whereas Fe as well as Mo and Ru were retained. The Zr elution was evaporated until the total volume reached ∼1 mL and then converted to 3 mL of ∼2 mol L^{-1} HCl solution by dilution with H$_2$O. The solution was loaded onto a column packed with Eichrom Ln-Spec resin (100–150 μm). Following that, Ti and Cr were removed from the column with 2 mol L^{-1} HNO$_3$ + 1 wt.% H$_2$O$_2$, and the matrix elements were eluted with 3 mol L^{-1} and 6 mol L^{-1} HCl, as well as 0.5 mol L^{-1} HNO$_3$. Subsequently, Zr was eluted with 0.5 mol L^{-1} HCl + 0.06 mol L^{-1} HF. The two-step ion-exchange chemistry was repeated with smaller resin volumes of ∼0.5 mL for all samples except for whole-rock fraction #1-1, orthopyroxene fractions #2-1 and #3, and chromite fractions #2-1 and #2-2.

All separated Zr fractions were treated with concentrated HF, HNO$_3$, and HClO$_4$ to decompose the organic matter. Finally, the Zr fractions were redissolved in 0.5 mol L^{-1} HNO$_3$ + trace HF solution and diluted to ∼10 ppb. The yields of the chemical separation procedure were more than 60%. When the Parr bomb was used for sample digestion, the total procedural Zr blanks, including sample dissolution and chemical separation, were 800–1300 pg and ∼20–40 pg for all other samples.

A.1.3. Zr Isotope Measurement Using MC-ICP–MS

The Zr isotope compositions were measured using a Thermo Fisher Scientific Neptune Plus MC-ICP–MS interfaced to a Cetac Aridus II desolvating nebulizer at the University of Tokyo. The measurements were conducted using a Jet sample cone and a skimmer H-cone in the low-resolution mode, which resulted in a typical Zr sensitivity of 0.60–0.85 V ppb^{-1} (10^{11}
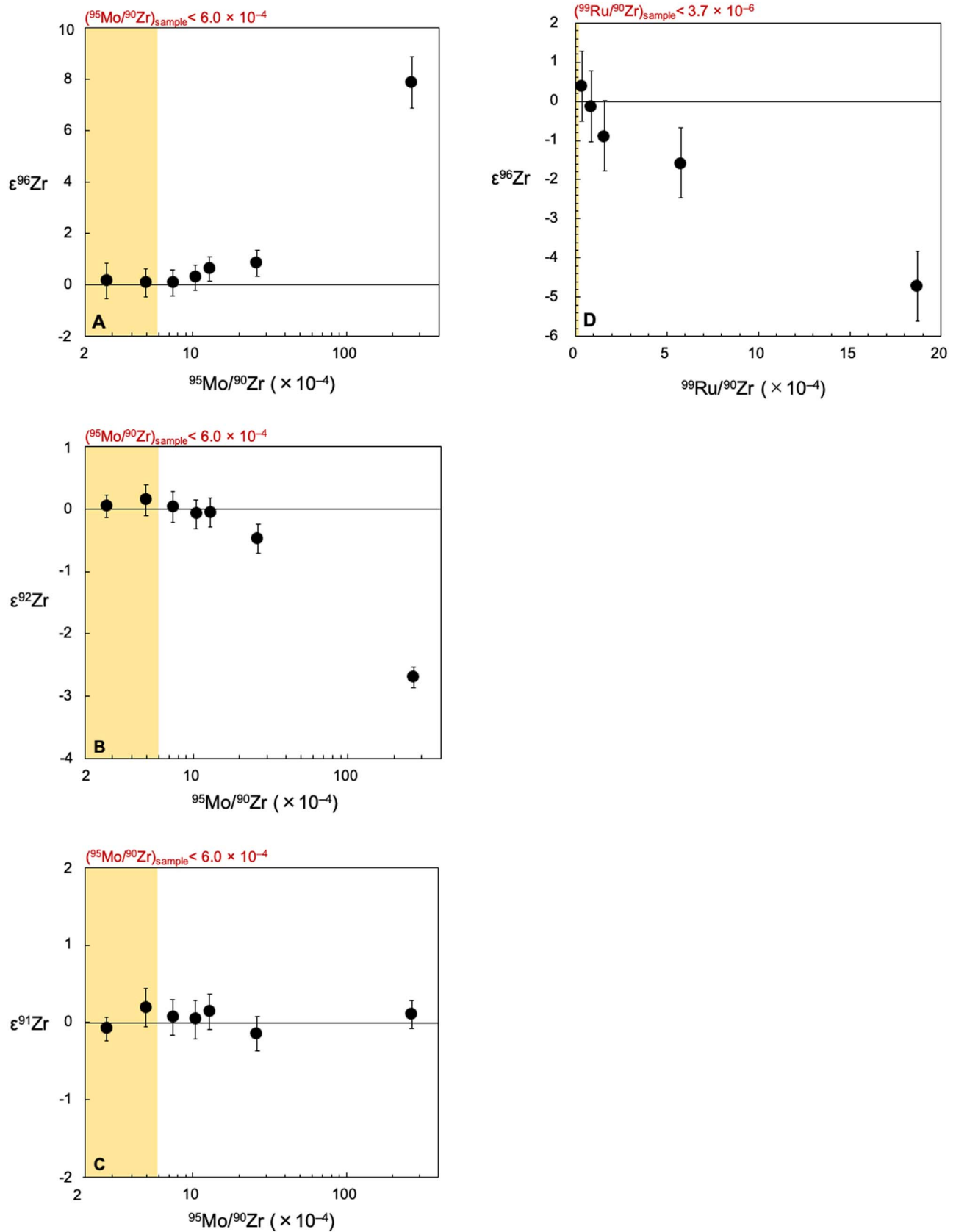
Figure A1. Zirconium isotope ratios after interference corrections for ((a)–(c)) Mo- and (d) Ru-doped NIST SRM 3169 Zr standard solutions. Each data point represents a single measurement. The error bars represent 2σ. The yellow bands indicate the ranges of the measured isotopic ratios for samples analyzed in this study. The ^{95}Mo/^{90}Zr and ^{99}Ru/^{90}Zr ratios of our sample solutions after purification are smaller than the accurate correction limits.
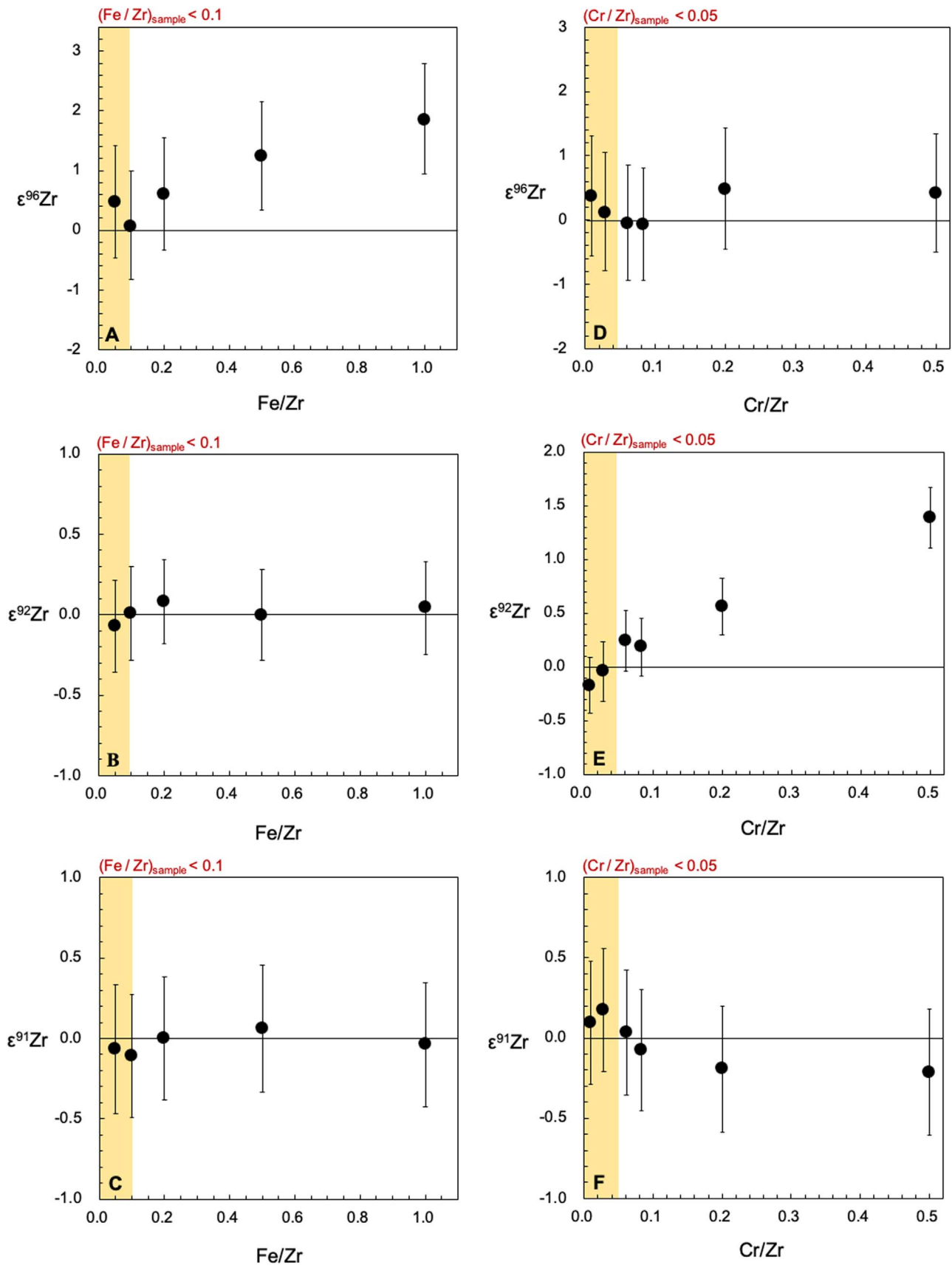
Figure A2. Zirconium isotope ratios measured for ((a)–(c)) Fe-, ((d)–(f)) Cr-, and ((g)–(i)) Ti-doped NIST SRM 3169 Zr standard solutions. Each data point represents a single measurement. The error bars represent 2σ. The yellow bands indicate the ranges of the samples used for the discussion in this study.
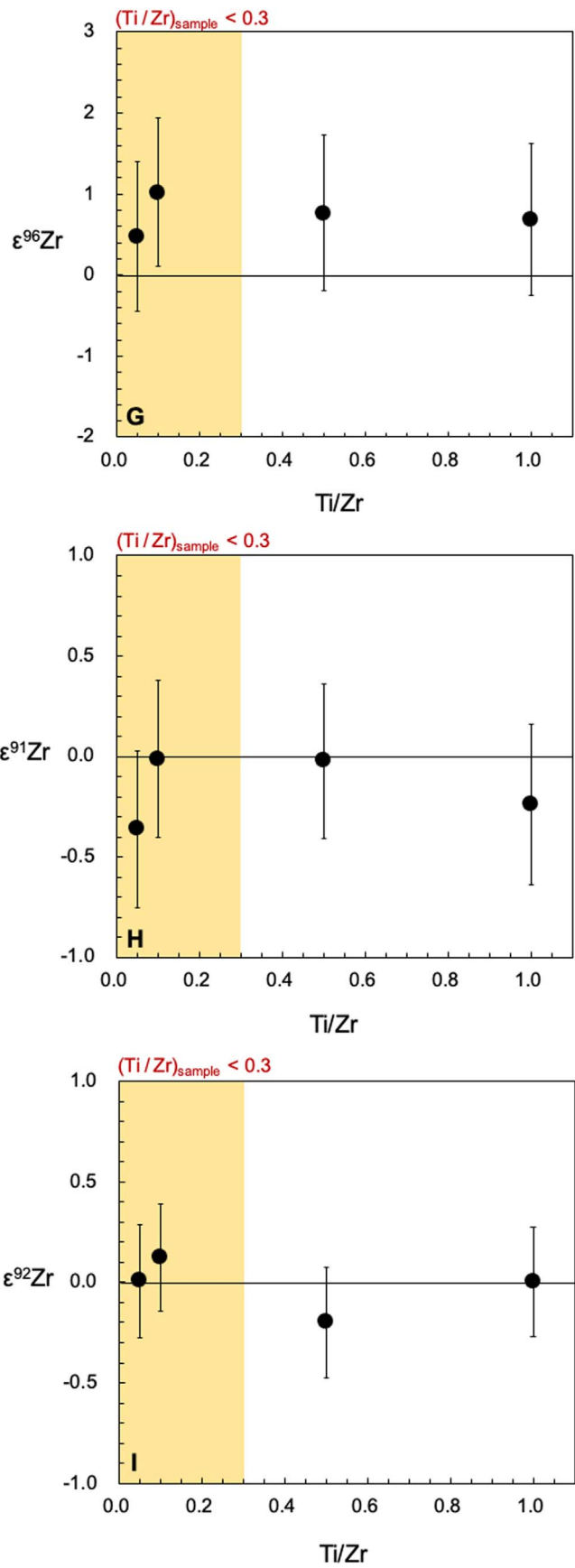
Figure A2. (Continued.)

Table A1
Nb–Zr Isotope Data for NWA 6704

Sample	Weight (mg)	Zr (ppm)	93Nb/90Zr ± 2σ	ε91Zr ± 2σ	ε92Zr ± 2σ	ε96Zr ± 2σ
Whole rock #1-1	48.3	3.8	0.26 ± 0.044	0.11 ± 0.23	0.02 ± 0.17	1.11 ± 0.62
Whole rock #1-2	49.5	3.5	0.23 ± 0.013	0.04 ± 0.18	0.07 ± 0.18	1.30 ± 0.72
Orthopyroxene #2-1	40.6	3.4	0.27 ± 0.044	0.13 ± 0.27	−0.02 ± 0.25	1.02 ± 0.57
Orthopyroxene #2-2	48.9	3.1	0.21 ± 0.013	0.01 ± 0.18	0.00 ± 0.19	1.08 ± 0.71
Orthopyroxene #3	27.7	4.2	0.21 ± 0.044	0.06 ± 0.25	0.13 ± 0.25	[a]1.97 ± 0.52
Orthopyroxene #4	49.1	3.4	0.25 ± 0.013	−0.04 ± 0.22	0.00 ± 0.24	1.45 ± 0.49
Chromite #2-1	4.1	14.6	1.26 ± 0.040	0.00 ± 0.48	1.18 ± 0.41	1.31 ± 0.87
Chromite #2-2	3.8	11.9	1.70 ± 0.040	−0.18 ± 0.47	1.20 ± 0.40	[a]4.52 ± 0.86
Chromite #3	2.9	17.8	1.91 ± 0.040	0.26 ± 0.31	1.33 ± 0.26	2.40 ± 1.37
Chromite #4-1	7.6	15.2	1.88 ± 0.012	0.02 ± 0.17	1.49 ± 0.18	1.89 ± 0.72
Chromite #4-2	6.5	15.5	2.09 ± 0.012	−0.06 ± 0.17	1.51 ± 0.17	2.23 ± 0.70
Chromite #5	6.5	8.0	1.12 ± 0.013	−0.08 ± 0.16	0.56 ± 0.20	[a]1.60 ± 0.69
Metal #4	165	2.2	0.22 ± 0.013	−0.05 ± 0.17	0.05 ± 0.18	1.79 ± 0.70

Note.
[a] The ε^{96}Zr values obtained for these samples were not used for the discussion because their high Fe/Zr ratios could hamper accurate ^{96}Zr measurements.

Ω resistor) at a sample uptake rate of $\sim$100 μL minute^{-1}. Data were acquired using Faraday cups in the static mode to monitor the isotopes ^{90}Zr, ^{91}Zr, ^{92}Zr, ^{94}Zr, and ^{96}Zr as well as ^{95}Mo and ^{99}Ru. Each sample measurement consisted of 60 cycles with an integration time of 8.4 s, which was preceded by an acid blank analysis of 30 cycles with the same integration time. The acid blank analysis was used for an on-peak-zero baseline subtraction. Instrumental mass fractionation was corrected relative to ^{94}Zr/^{90}Zr = 0.3381 (Minster & Allègre 1982) using an exponential law. Following a previously reported protocol, the isobaric interferences of ^{92,94}Mo on ^{92,94}Zr and ^{96}Mo and ^{96}Ru on ^{96}Zr were corrected (Schönbächler et al. 2004). To evaluate the accuracy of the interference correction methods, we ran Zr standard solutions variably doped with Mo and Ru. The results indicate that the correction methods are robust for ^{91}Zr/^{90}Zr and ^{92}Zr/^{90}Zr in samples with a Mo/Zr reaching up to 0.005 and for ^{96}Zr/^{90}Zr in samples with Mo/Zr and Ru/Zr reaching up to 0.004 and 0.0007, respectively (Figure A1). As the isobaric interference of ^{96}Ru on ^{96}Zr was negligibly small in all samples separated in this study, a correction for Ru was not carried out. We also checked the effects of argide interferences on the Zr isotope measurements by analyzing Zr standard solutions doped with Fe, Cr, and Ti. The results show that the measured ^{96}Zr/90Zr and ^{92}Zr/^{90}Zr ratios are inaccurate when the Fe/Zr and Cr/Zr ratios are higher than 0.2 and 0.1, respectively.

Each sample measurement was bracketed by an analyses of a 10 ppb Zr standard solution of the National Institute of Standards and Technology (NIST) Standard Reference Material (SRM) 3169. The signal intensity of ^{90}Zr was 3–4 V for a 10 ppb solution, and approximately 10 ng of Zr was consumed in one analysis. All the Zr isotope ratios of the samples in Table A1 are expressed as relative deviations from the standard analyses in the same analytical session using the epsilon notation:

$$\varepsilon^x\mathrm{Zr} = \left(\left[\frac{{}^x\mathrm{Zr}}{{}^{90}\mathrm{Zr}} \right]_{\mathrm{Sample}} \Big/ \left[\frac{{}^x\mathrm{Zr}}{{}^{90}\mathrm{Zr}} \right]_{\mathrm{Standard}} - 1 \right) \times 10^4. \quad \text{(A1)}$$

Analytical uncertainties in the sample Zr isotope ratios include the internal precision (two standard errors, or 2SE) and reproducibility of standard analyses (two standard deviations, or 2SD), added in quadrature.

A.1.4. Nb/Zr Measurement Using ICP–MS

The sample aliquots for the ^{93}Nb/^{90}Zr analyses were evaporated and redissolved in 0.5–2 mL of 0.5 mol L^{-1} HNO$_3$ + trace HF solution without chemical separation. The analyses were carried out at the University of Tokyo using a Thermo Fisher Scientific iCAP Q ICP–MS. The instrument was operated in kinetic energy discrimination (KED) mode using He as the collision gas. This significantly suppresses the production of Cr-and Ti-argide ions that interfere with Nb and Zr ions; the production rate of Ti-argide (^{50}Ti^{40}Ar/^{50}Ti) was $\leqslant 8.0 \times 10^{-5}$ and that of Cr-argide (^{52}Cr^{40}Ar/^{52}Cr) was $\leqslant 2.0 \times 10^{-6}$, leading to negligible argide interferences. The samples were introduced to the ICP–MS using the Cetac Aridus II desolvating nebulizer (whole-rock #1–1, orthopyroxenes #2–1 and #3, and chromites #2–1, #2–2, and #3) or a cyclonic spray chamber (all other samples). The instrumental Nb/Zr fractionation correction was performed by using multiple measurements of standard solutions. To evaluate the effect of the sample matrix on the Nb/Zr fractionation, we prepared three working standard solutions containing 0.5 ppb Nb and Zr: (i) STD-Chr, a solution doped with 10 ppm Cr, 5 ppm Fe, and 1 ppm Ti, similar to the matrix of chromite sample solutions; (ii) STD-Px, a solution doped with 100 ppm Fe, 50 ppm Mg, 1 ppm Cr, and 0.3 ppm Ti, similar to pyroxene and whole-rock sample solutions; and (iii) STD-W/O, an undoped solution. Analyses of these standard solutions yielded identical Nb/Zr fractionation factors within the uncertainty when the spray chamber was used. When the desolvating nebulizer was utilized, the fractionation factor of STD-Chr was 4% lower than that of STD-Px and 6% higher than that of STD-W/O. Thus, we applied the STD-Chr fractionation factor to the chromite samples and the STD-Px fractionation factor to the remaining samples. Analytical uncertainties in the sample ^{93}Nb/^{90}Zr ratios (Table A1) include the internal 2SE of each sample and the 2SD of repeated standard measurements. To account for the imperfect matrix matching between the standard and sample solutions, a 4% error (difference in the fractionation

Table A2
Zirconium Column Chromatography

Step	Volume (mL)	Acid
Column 1 (2 mL AG1-X8 anion resin 200–400 mesh $d = \sim6.5$ mm, $h = 54$ mm)		
Load	2	6 mol L–1 HCl
Collect Zr	4	6 mol L–1 HCl
Column 2 (2.5 mL Ln-Spec resin 100–150 μm $d = \sim2.4$ mm, $h = 20$ cm)		
Load sample	3	3 mol L–1 HNO3
Ti, Cr, Fe, Mo, Ru removal	30.5	2 mol L–1 HNO3—1 wt.% H2O2
Residual Fe, Mo, removal	1	0.5 mol L–1 HNO3
Residual Fe, Mo, removal	5	3 mol L–1 HCl
Rinse	5	6 mol L–1 HCl
Rinse	1	0.5 mol L–1 HNO3
Rinse	2	0.5 mol L–1 HCl—0.06 mol L–1 HF
Collect Zr	16	0.5 mol L–1 HCl—0.06 mol L–1 HF
Additional 1 (0.5 mL AG1-X8 anion resin 200–400 mesh $d = \sim2$ mm, $h = 30$ mm)		
Load sample & collect Zr	0.2	6 mol L–1 HCl
Collect Zr	1.5	6 mol L–1 HCl
Additional 2 (0.5 mL Ln-Spec resin 100–150 μm $d = \sim2$ mm, $h = 30$ mm)		
Load sample	0.2	2 mol L–1 HCl
Ti, Cr, Fe, Mo, Ru removal	6	2 mol L–1 HNO3—1 wt.% H2O2
Residual Fe, Mo, removal	0.1	0.5 mol L–1 HNO3
Residual Fe, Mo, removal	0.5	3 mol L–1 HCl
Rinse	1	6 mol L–1 HCl
Rinse	0.1	0.5 mol L–1 HNO3
Collect Zr	4	0.5 mol L–1 HCl—0.06 mol L–1 HF

factor between STD-Chr and STD-Px) was propagated for the samples measured with the desolvating nebulizer.

A.1.5. Evaluation of Data

To evaluate the effectiveness of the chemical separation, the elemental abundances of the separated Zr fractions were determined using the iCAP QTM ICP–MS. The results reveal that the residual abundances of the elements causing spectral interferences are lower in most sample fractions than the upper limits of accurate Zr isotope analysis (Figures A1, A2). The only exceptions are orthopyroxene fraction #3, chromite fraction #2–2, and chromite fraction #5 (Fe/Zr = 0.22–0.43), for which the two-step ion-exchange chemistry was not repeated. Such elevated Fe abundances may impede accurate determination of ε^{96}Zr (Figures A2(A)–(C)). In fact, chromite #2–2 yielded a significantly higher ε^{96}Zr than the other fractions. Hence, the ε^{96}Zr values obtained from these fractions were excluded from the discussion. The remaining ε^{96}Zr values are identical within the analytical uncertainty and yield a mean value of 1.56 ± 0.98 (2SD). It should be noted that the elevated Fe levels have negligible effect on the determination of ε^{91}Zr and ε^{92}Zr (Figures A2(B)–(C)).

ORCID iDs

Yuki Hibiya ⓘ https://orcid.org/0000-0002-3346-9820
Tsuyoshi Iizuka ⓘ https://orcid.org/0000-0001-7896-5812
Takehito Hayakawa ⓘ https://orcid.org/0000-0001-5286-8395

References

Akram, W., Schönbächler, M., Bisterzo, S., et al. 2015, GeCoA, 165, 484
Amelin, Y., Koefoed, P., Iizuka, T., et al. 2019, GeCoA, 245, 628
Blinova, A., Amelin, Y., & Samson, C. 2007, M&PS, 42, 1337
Bollard, J., Kawasaki, N., Sakamoto, N., et al. 2019, GeCoA, 260, 62
Brennecka, G. A., Burkhardt, C., Budde, G., et al. 2020, Sci, 370, 837
Connelly, J. N., Bizzarro, M., Krot, A. N., et al. 2012, Sci, 338, 651
Cook, D. L., Clayton, R. N., Wadhwa, M., et al. 2008, GeoRL, 35, L01203
Côté, B., Lugaro, M., Reifarth, R., et al. 2019, ApJ, 878, 156
Dauphas, N., Rauscher, T., Marty, B., et al. 2003, NuPhA, 719, C287
Diehl, R., Halloin, H., Kretschmer, K., et al. 2006, Natur, 439, 45
Dwarkadas, V. V., Dauphas, N., Meyer, B., et al. 2017, ApJ, 851, 147
Fang, L., Frossard, P., Boyet, M., et al. 2022, PNAS, 119, 12
Gaidos, E., Krot, A. N., Williams, J. P., et al. 2009, ApJ, 696, 1854
Haba, M. K., Lai, Y. J., Wotzlaw, J. F., et al. 2021, PNAS, 118, 2017750118
Haba, M. K., Wotzlaw, J. F., Lai, Y. J., et al. 2019, NatGeo, 12, 510
Harper, C. L., Jr 1996, ApJL, 466, L437
Hayakawa, T., Nakamura, K., Kajino, T., et al. 2013, ApJL, 779, L9
Hibiya, Y., Archer, G. J., Tanaka, R., et al. 2019, GeCoA, 245, 597
Hirata, T. 2001, ChGeo, 176, 323
Holden, N. E. 1990, PApCh, 62, 941
Holst, J. C., Olsen, M. B., Paton, C., et al. 2013, PNAS, 110, 8819
Huss, G. R., Meyer, B. S., Srinivasan, G., et al. 2009, GeCoA, 73, 4922
Iizuka, T., Amelin, Y., Kaltenbach, A., et al. 2014, GeCoA, 132, 259
Iizuka, T., Jourdan, F., Yamaguchi, A., et al. 2019, GeCoA, 267, 275
Iizuka, T., Lai, Y. J., Akram, W., et al. 2016, E&PSL, 439, 172
Jochum, K. P., Seufert, H. M., Spettel, B., et al. 1986, GeCoA, 50, 1173
Kastner, J. H., & Myers, P. C. 1994, ApJ, 421, 605
Kleine, T., Hans, U., Irving, A. J., et al. 2012, GeCoA, 84, 186
Leya, I., Schönbächler, M., Wiechert, U., et al. 2008, E&PSL, 266, 233
Lodders, K., Palme, H., & Gail, H. P. 2009, LanB, 4B, 712
Lugaro, M., Heger, A., Osrin, D., et al. 2014, Sci, 345, 650
Lugaro, M., Pignatari, M., Ott, U., et al. 2016, PNAS, 113, 907
Meyer, B. S. 2003, NuPhA, 719, C13
Meyer, B. S. 2005, in ASP Conf. Ser. 341, Chondrites and the Protoplanetary Disk, ed. A. N. Krot, E. R. D. Scott, & B. Reipurth (San Francisco: ASP), 515
Minster, J. F., & Allègre, C. J. 1982, GeCoA, 46, 565
Münker, C., Fonseca, R. O., & Schulz, T. 2017, NatGeo, 10, 822
Münker, C., Weyer, S., Mezger, K., et al. 2000, Sci, 289, 1538
Münker, C., Weyer, S., Scherer, E., et al. 2001, GGG, 2, 1064
Qin, L., Carlson, R. W., & Alexander, C. M. D. 2011a, GeCoA, 75, 7806
Render, J., Brennecka, G. A., Burkhardt, C., et al. 2022, E&PSL, 595, 117748
Sahijpal, S., & Soni, P. 2006, M&PS, 41, 953
Sanborn, M. E., Wimpenny, J., Williams, C. D., et al. 2019, GeCoA, 245, 577
Sanloup, C., Blichert-Toft, J., Télouk, P., et al. 2000, E&PSL, 184, 75
Schiller, M., Bizzarro, M., & Fernandes, V. A. 2018, Natur, 555, 507
Schiller, M., Connelly, J. N., Glad, A. C., et al. 2015, E&PSL, 420, 45

Schönbächler, M., Lee, D. C., Rehkämper, M., et al. 2003, E&PSL, 216, 467
Schönbächler, M., Rehkamper, M., Halliday, A. N., et al. 2002, Sci, 295, 1705
Schönbächler, M., Rehkämper, M., Lee, D. C., et al. 2004, Ana, 129, 32
Sieverding, A., Martínez-Pinedo, G., Huther, L., et al. 2018, ApJ, 865, 143
Tatischeff, V., Duprat, J., & de Seéréville, N. 2010, ApJL, 714, L26
Travaglio, C., Gallino, R., Rauscher, T., et al. 2014, ApJ, 795, 141

Warren, P. H. 2011, EPSL, 311, 93
Wasserburg, G. J., Busso, M., Gallino, R., et al. 2006, NuPhA, 777, 5
Wimpenny, S. M. E., Sanborn, M. E., Koefoed, P., et al. 2019, GeCoA, 244, 478
Yin, Q. Z., Jacobsen, S. B., McDonough, W. F., et al. 2000, ApJL, 536, L49
Young, E. D. 2016, ApJ, 826, 129